International Journal of Solids and Structures 47 (2010) 126–137

Contents lists available at ScienceDirect

International Journal of Solids and Structures

journal homepage: www.elsevier.com/locate/ijsolstr

Damage analysis and dynamic response of elasto-plastic laminated composite shallow spherical shell under low velocity impact

Fu Yiming, Mao Yiqi *, Tian Yanping

State Key Lab. of Advanced Technology of Design and Manufacturing for Vehicle Body, Hunan University, PR China
College of Mechanics and Aerospace, Hunan University, Changsha 410082, China

ARTICLE INFO

Article history:
Received 26 June 2009
Received in revised form 4 September 2009
Available online 18 September 2009

Keywords:
Low velocity impact
Elasto-plastic contact
Shallow spherical shell
Damage
Nonlinear dynamic response

ABSTRACT

Based on the elasto-plastic mechanics, the damage analysis and dynamic response of an elasto-plastic laminated composite shallow spherical shell under low velocity impact are carried out in this paper. Firstly, a yielding criterion related to spherical tensor of stress is proposed to model the mixed hardening orthotropic material, and accordingly an incremental elasto-plastic damage constitutive relation for the laminated shallow spherical shell is founded when a strain-based Hashin failure criterion is applied to assess the damage initiation and propagation. Secondly, using the presented constitutive relations and the classical nonlinear shell theory, a series of incremental nonlinear motion equations of orthotropic moderately thick laminated shallow spherical shell are obtained. The questions are solved by using the orthogonal collocation point method, Newmark method and iterative method synthetically. Finally, a modified elasto-plastic contact law is developed to determine the normal contact force and the effect of damage, geometrical parameters, elasto-plastic contact and boundary conditions on the contact force and the dynamic response of the structure under low velocity impact are investigated.

1. Introduction

Fiber-reinforced composite materials are extensively applied to the structures' manufactures in modern industries recently. These composite structures are susceptible to impact which inevitably exists in the transportation and application. So the forecast of the damage and impact response of these structures is of great practical benefit to their design and manufacture.

The impact event is a complex phenomenon which includes the interaction between projectile and structure. Recently, lots of researches on impact have been carried out in experimental and numerical form. When only the elastic contact is in consideration, Yang and Sun (1981) presented the experimental indentation law through static indentation tests on composite laminates; Tam and Sun (1982) developed their own finite program to analyze impact response of composite laminates and performed impact tests by using a pendulum type low velocity impact test system; Sun (1977) applied the modified Hertzian contact law to the dynamic analysis of the composite laminates under impact; Choi and Lim (2004) proposed a linearized contact law in low velocity impact analysis of composite laminates and compared it to the modified Hertzian contact law. When the plastic deformation occurs in contact area as the deflection of the structure under impact increases, the elastic contact law is no longer suitable to model the contact force and a more feasible contact law is needed. So Johnson (1985) applied the Hertzian theory and Von Mises yield criterion to determine the normal force at which the incipient yield occurs in two spheres subjected to a normal load. Chang et al. (1987) proposed the CEB (Chang, Etsion and Bogy) model in the analysis of composite laminates under impact of a sphere. In this model the sphere remains in elastic Hertzian contact until a critical interference is reached, above which volume conservation of the sphere tip is imposed. The contact pressure distribution for the plastic deformed composite laminates structures was assumed to be rectangular and equal to the maximum Hertzian pressure at critical interference. The CEB model suffers from a discontinuity in contact load as well as in the first derivatives of both contact load and contact area at the transition from the elastic to the elasto-plastic regime. Vu-Quoc and Zhang (1999), Vu-Quoc et al. (2001, 2000) made further advance in the theory and numerical analysis, and proposed an accurate elasto-plastic NFD (normal force–displacement) model, which had been experimentally validated in Plantard and Papini (2005). But this model is only suitable to the elasto-perfectly plastic material. So, we attempt in the present paper to establish an elasto-plastic contact law based on the elasto-perfectly plastic NFD (normal force–displacement) model presented in Vu-Quoc et al. (2001). However, only the case of normal impact is investigated in this paper, and the oblique impact, a more general and realistic case, can refer to Vu-Quoc et al. (2004), Zhang

* Corresponding author. Address: State Key Lab. of Advanced Technology of Design and Manufacturing for Vehicle Body, Hunan University, Changsha, Hunan 410082, PR China. Tel.: +86 013574188814; fax: +86 731 8822051.
E-mail address: maoyiqi1984@163.com (M. Yiqi).

0020-7683/$ - see front matter © 2009 Elsevier Ltd. All rights reserved.
doi:10.1016/j.ijsolstr.2009.09.017

and Vu-Quoc (2007), in which a tangential elasto-plastic force–displacement model had been developed.

Invisible damages of various kinds are easy to be induced in composite laminates when impacted by projectiles, such as: delamination, matrix crack and fiber breakage. They would heavily reduce the stiffness and life-span of the structures. Experiments show that composite materials are more susceptible to the impact than the metal. So a full comprehension of the damage mechanism for composite laminates under low velocity impact is very important. Collombet et al. (1996) presented some numerical tools to simulate the low velocity impact damage of laminated composite structures. They considered a model of contact-impact based on Lagrange multiplier technique. Matrix cracking is represented by an averaging technique developed on the scale of one finite element. The results showed good agreement between the experimental and numerical damage observations. Choi and Chang (1992) used the dynamic finite element method coupled with failure analysis to predict the threshold of impact damage and initiation of delamination. Hou et al. (2000) predicted the impact damage for laminated composites with implementation of an improved failure criterion, suggesting that delamination was constrained by the through-thickness compression stress; Ganapathy and Rao (1997) predicted the damage in laminated composite plates and in cylindrical/spherical shell panels subjected to low velocity impact. The in-plane damage in the laminates was firstly analyzed by a 2D nonlinear finite element model using laminated composite shell elements with a 48 degree-of-freedom. The in-plane damage was then analyzed by using the Tsai–Wu criterion and maximum stress criteria.

In this paper, an elastic progressive stiffness modification method is established by adopting the strain-based Hashin failure criterion at first, and then an elasto-plastic constitutive relation for orthotropic materials containing damage are built when the yield criterion related to spherical tensor of stress is proposed to describe the mixed hardening of damaged orthotropic materials. Based on the nonlinear classical flat shell theory, the incremental nonlinear motion equations of orthotropic moderately thick shallow spherical shells are obtained. With the previously deduced yield criterion related to spherical tensor of stress, we developed the Vu-Quoc et al. (2000) elasto-perfectly plastic contact model to model the contact force and indentation in the plastic loading phase. Numerical results show the effect of damage, geometrical parameters of the structure and boundary conditions on the contact force and the dynamic response of the structure under low velocity impact.

2. Basic equations

2.1. Incremental nonlinear geometric relations for the laminated composite shallow spherical shell

Consider an axi-symmetrical laminated moderately thick shallow spherical shell with the thickness h, the number of the plies N and base radius a. The shell is impacted by an elastic sphere on the top with a velocity of v_0 (as shown in Fig. 1). Each point in the shells can be denoted with the orthogonal curvilinear coordinates φ, θ, z along the meridional, circumferential and radial/thickness directions, respectively. $z = 0$ denotes the mid-surface and $z = \pm h/2$ denote the inner and outer surfaces of the laminated shallow spherical shell, respectively. The curvature radius of the mid-surface is $R_1 = R_2 = R$, and the Lame coefficients are $A_1 = R, A_2 = R\sin\varphi$. Under the *Timoshenko–Midlin* assumption, the incremental displacement components du, dv, dw of any point in the shell at any time for the axi-symmetrical deformation can be expressed as

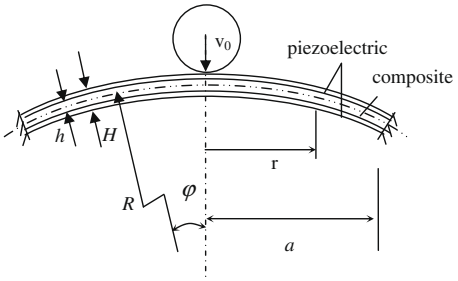

Fig. 1. Geometrical configuration of the shallow spherical shell with fixed boundary.

$$\begin{aligned} du(\varphi,\theta,z,t) &= du^0(\varphi,\theta,t) + zd\psi_1(\varphi,\theta,t) \\ dv(\varphi,\theta,z,t) &= 0 \\ dw(\varphi,\theta,z,t) &= dw^0(\varphi,\theta,t) \end{aligned} \tag{1}$$

where du^0, dw^0 are the incremental displacement components on the mid-surface of the laminated shallow spherical shell; $d\psi_1$ is the incremental independent rotation of the radial section. The nonlinear incremental strain–displacement relations are expressed as follows

$$d\varepsilon_\varphi = d\varepsilon_\varphi^0 + zdk_\varphi^0, \quad d\varepsilon_\theta = d\varepsilon_\theta^0 + zdk_\theta^0, \quad d\varepsilon_{\varphi z} = d\psi_1 + \frac{1}{R}\frac{\partial dw}{\partial\varphi} \tag{2}$$

where $d\varepsilon_\varphi^0, d\varepsilon_\theta^0$ are the incremental strain components on the mid-surface, $dk_\varphi^0, dk_\theta^0$ are the changes of the curvatures on the mid-surface, and

$$\begin{aligned} d\varepsilon_\varphi^0 &= \frac{1}{R}\frac{\partial du^0}{\partial\varphi} - \frac{dw}{R} + \frac{1}{2}(d\omega_2)^2 + \omega_2\cdot d\omega_2, \\ d\varepsilon_\theta^0 &= \frac{\cot\varphi}{R}du^0 - \frac{dw}{R}, \quad k_\varphi^0 = \frac{1}{R}\frac{\partial d\psi_1}{\partial\varphi}, \quad k_\theta^0 = \frac{\cot\varphi}{R}d\psi_1 \end{aligned} \tag{3}$$

in which ω_2 is rotational component and $\omega_2 = -\frac{1}{2}\left(\frac{1}{R}\frac{\partial w}{\partial\varphi} - \psi_1\right)$, $d\omega_2 = -\frac{1}{2}\left(\frac{1}{R}\frac{\partial dw}{\partial\varphi} - d\psi_1\right)$.

In the analysis of the shallow spherical shell, a new variable r is introduced in the radius of the parallel circle, and then there exist the following relation $r \approx R\varphi, \sin\varphi, \cos\varphi \approx 1$ approximately. Therefore, according to Eq. (3), the incremental strain and rotary angle components can be simply expressed as

$$\begin{aligned} d\varepsilon_\varphi^0 &= \frac{\partial du^0}{\partial r} - \frac{dw}{R} + \frac{1}{2}(d\omega_2)^2 + \omega_2\cdot d\omega_2, \\ d\varepsilon_\theta^0 &= \frac{du^0}{r} - \frac{dw}{R}, \quad dk_\varphi^0 = \frac{\partial d\psi_1}{\partial r}, \quad dk_\theta^0 = \frac{d\psi_1}{r}, \\ \omega_2 &= -\frac{1}{2}\left(\frac{\partial w}{\partial r} - \psi_1\right), \quad d\omega_2 = -\frac{1}{2}\left(\frac{\partial dw}{\partial r} - d\psi_1\right) \end{aligned} \tag{4}$$

2.2. Incremental elastic damage constitutive relations for orthotropic composite shallow spherical shell

According to Zhang et al. (2006), Chien and Lee (2003), when the orthotropic composite structures are subjected to a low velocity impact, the stiffness coefficients would be reduced when the failure thresholds are reached and would be reduced further as deformation increases. After the stiffness coefficients are firstly degraded at a local point, the stresses may become chaotic while strains are more continuous and would be basis better suited to assess failure. On the basis of the damage model presented by Zhang et al. (2006), and for the axi-symmetrical deformation analysis, three failure symbols, s_1, s_2 and s_3 are defined as follows

Strain-based fiber failure

$$\begin{aligned} s_1 &= \tfrac{\varepsilon_{11}}{X_c^\varepsilon}, \quad \varepsilon_{11} < 0 \\ s_1 &= \tfrac{\varepsilon_{11}}{X_T^\varepsilon}, \quad \varepsilon_{11} \geqslant 0 \end{aligned} \tag{5}$$

Strain-based matrix failure

$$\begin{aligned} s_2 &= \tfrac{E_2^2}{4G_{23}^2}\left(\tfrac{\varepsilon_{22}}{T_{23}^\varepsilon}\right)^2 + \tfrac{\varepsilon_{22}}{Y_c^\varepsilon}\left[\tfrac{E_2^2}{4G_{23}^2}\left(\tfrac{Y_c^\varepsilon}{T_{23}^\varepsilon}\right)^2 - 1\right] + \left(\tfrac{\gamma_{13}}{T_{13}^\varepsilon}\right)^2, \quad \varepsilon_{22} < 0 \\ s_2 &= \left(\tfrac{\varepsilon_{22}}{Y_T^\varepsilon}\right)^2 + \left(\tfrac{\gamma_{13}}{T_{13}^\varepsilon}\right)^2, \qquad\qquad\qquad\qquad \varepsilon_{22} \geqslant 0 \end{aligned} \tag{6}$$

Strain-based fiber–matrix shear failure

$$s_3 = \left(\frac{\langle -\varepsilon_{11}\rangle}{X_c^\varepsilon}\right)^2 + \left(\frac{\gamma_{13}}{T_{13}^\varepsilon}\right)^2 \tag{7}$$

The MaCauley arithmetic sign $\langle\cdot\rangle$ is defined as:

$$\langle l\rangle = \begin{cases} l & \text{if } l > 0 \\ 0 & \text{if } l \leqslant 0 \end{cases} \tag{8}$$

where E_1 and E_2 are the Young's modulus along and perpendicular to the fiber direction, respectively, $G_{ij}(i \neq j)$ are the corresponding shear stiffness constants in the ij-plane; $X_c^\varepsilon, X_T^\varepsilon, Y_c^\varepsilon, Y_T^\varepsilon$ are the compression and tension strain strength along and perpendicular to the fiber direction, and they can be obtained by substitution of only one dimension relations as follows

$$X_T^\varepsilon = \frac{X_T}{E_1}, \quad X_C^\varepsilon = \frac{X_c}{E_1}, \quad Y_T^\varepsilon = \frac{Y_T}{E_2}, \quad Y_C^\varepsilon = \frac{Y_c}{E_2}, \quad T_{ij}^\varepsilon = \frac{T_{ij}}{G_{ij}} \tag{9}$$

where X_C, X_T, Y_C and Y_T are the compression and tension strength along and perpendicular to the fiber direction, and T_{ij} represents the shear strength in the ij-plane. With the above transformation, the three symbols based on the strain-based Hertzian law can be used to reflect the damage degree in the structures (when $s_i > 1,\ i = 1,2,3$). In order to evaluate the damage in the composite materials, three failure variables (d_1, d_2, d_3) are defined in terms of the damage symbols (s_1, s_2, s_3) as:

$$d_i = \kappa_i\left(1 - \frac{A_i}{s_i^n}\right) \quad (i = 1,2,3) \tag{10}$$

where $\kappa(0 < \kappa_i \leqslant 1),\ n$ and A are damage parameters.

The span of damage variables are $[0,1]$, $d = 0$ indicates no damage, $d = 1$ indicates the completely material failure. As the damage variables are time-dependent and un-restored, the damage variables are supposed to meet the following condition

$$d^t = \max(d^\tau, 0)(\tau \leqslant t), \quad d^0 = 0 \tag{11}$$

The material constants $\mathbf{H}$ without damage can be related to the damaged material constants $\mathbf{H}'$ as follows

$$\mathbf{H}' = (\mathbf{I} - \mathbf{F}) \cdot \mathbf{H} \tag{12}$$

where $\mathbf{F}$ is a diagonal matrix with diagonal components d_1, d_2 and d_3, and $\mathbf{H} = (E_1, E_2, G_{13})^T,\ \mathbf{H}' = (E_1', E_2', G_{13}')^T$.

Then, the constitutive relations for the kth lamina of the laminated shallow spherical shells containing damage can be expressed as

$$\begin{Bmatrix} d\sigma_\varphi^k \\ d\sigma_\theta^k \\ d\sigma_{\varphi z}^k \end{Bmatrix} = \begin{bmatrix} \frac{E_1^k(1-d_1^k)}{1-v_{12}^k v_{21}^k} & \frac{E_1^k(1-d_1^k)v_{21}^k}{1-v_{12}^k v_{21}^k} & 0 \\ \frac{E_1^k(1-d_1^k)v_{21}^k}{1-v_{12}^k v_{21}^k} & \frac{E_2^k(1-d_2^k)}{1-v_{12}^k v_{21}^k} & 0 \\ 0 & 0 & G_{13}^k(1-d_3^k) \end{bmatrix} \begin{Bmatrix} d\varepsilon_\varphi^k \\ d\varepsilon_\theta^k \\ d\varepsilon_{\varphi z}^k \end{Bmatrix} \stackrel{def}{=} \begin{bmatrix} c_{11}^k & c_{12}^k & 0 \\ c_{12}^k & c_{22}^k & 0 \\ 0 & 0 & c_{44}^k \end{bmatrix} \begin{Bmatrix} d\varepsilon_\varphi^k \\ d\varepsilon_\theta^k \\ d\varepsilon_{\varphi z}^k \end{Bmatrix} \tag{13}$$

where $\sigma_\varphi^k, \sigma_\theta^k, \tau_{\varphi z}^k$ are the stress components, $\varepsilon_\varphi^k, \varepsilon_\theta^k, \varepsilon_{\varphi z}^k$ are the strain components, d_1^k, d_2^k, d_3^k are the damage variables, E_1^k, E_2^k are the Young's modulus along and perpendicular to the fiber, respectively, G_{13}^k is the shear modulus in 1–3 plane; v_{12}^k, v_{21}^k are the Poisson's ratio and $E_1^k/v_{12}^k = E_2^k/v_{21}^k$, and the superscript k indicates that the variables are in the kth layer.

The Eq. (13) is simply denoted as

$$\mathbf{d}\boldsymbol{\sigma} = \mathbf{c}^e \cdot \mathbf{d}\boldsymbol{\varepsilon}^e \tag{14}$$

the superscript e indicates the elastic property.

2.3. Mixed hardening rule and elasto-plastic damage constitutive relations for orthotropic composite shallow spherical shell

2.3.1. Mixed hardening rule

For the axi-symmetry plane stress problem, in the case of elasto-plastic deformation, we suppose that:

(1) spherical tensors of stresses produce plastic deformations, and the plastic strains are compressible;
(2) uniform volume dilatation produced by the active stresses does not influence plastic deformation;
(3) yield surface moves and expands along with plastic deformation;
(4) dimensionless yield criterion of orthotropic material is isomorphic with the Von Mises criterion of isotropic material.

Based on above suppositions, the mixed hardening yield criterion of orthotropic damaged materials can be written as

$$F_p = f(\sigma_{ij} - b_{ij}) - k(\xi) \tag{15}$$

where $f(\sigma_{ij} - b_{ij})$ is the yield function; σ_{ij} is the stress components of the damaged material; b_{ij} is the back stress, which denotes the transition of the center of the yield surface and reflects the kinematic hardening; hardening parameter $k(\xi)$ denotes the size of yield surface, which is often set as equivalent active stress $\bar{\sigma}$, and ξ is an internal variable often set as equivalent plastic strain $\bar{\varepsilon}^p$ ($\bar{\sigma}$ and $\bar{\varepsilon}^p$ are both defined in the following).

To satisfy the supposition (2), the uniform volume dilatation caused by the stress components of the damaged material must meet $\varepsilon_{11} = \varepsilon_{22}$, here, $\frac{\sigma'_{11}}{c_{11}^e + c_{12}^e} = \frac{\sigma'_{22}}{c_{21}^e + c_{22}^e}$, and $\sigma'_{ij} = \sigma_{ij} - b_{ij},\ c_{ij}^e$ are defined in Eq. (14).

Supposing the principal directions of the material along the direction of x, y, z, the yield function $f(\sigma'_{ij})$ can be given as

$$f = k_{12}\left(\frac{\sigma'_{11}}{c_{11}^e + c_{12}^e} - \mu_{12}\frac{\sigma'_{22}}{c_{21}^e + c_{22}^e}\right)^2 + k_{23}\left(\frac{\sigma'_{22}}{c_{21}^e + c_{22}^e}\right)^2 + 2k_{44}\sigma_{44}'^2 \tag{16}$$

in which k_{ij}, μ_{ij} are constant coefficients need to be determined.

For the supposition (4), the following coefficients have been chosen by comparing to the Von Mises yield criterion

$$\begin{aligned} k_{12} &= \frac{(c_{11}^e + c_{12}^e)^2}{2S_{12}^2}, \quad k_{23} = \frac{(c_{21}^e + c_{22}^e)^2}{2S_{22}^2}, \\ \mu_{12} &= \frac{(c_{21}^e + c_{22}^e)}{(c_{11}^e + c_{12}^e)}\frac{S_{11}}{S_{22}}, \quad k_{44} = \frac{1}{2S_{44}^2} \end{aligned} \tag{17}$$

where S_{11} and S_{22} are yield stresses in the directions of principal axes x, y; S_{12} and S_{44} are yield pure shear stresses in the coordinate planes of (x, y) and (x, z), respectively. Then the dimensionless yield function can be written as

$$\bar{f} = \frac{1}{2}\left[(\bar{\sigma}'_{11} - \bar{\sigma}'_{22})^2 + \bar{\sigma}_{22}'^2 + \bar{\sigma}_{11}'^2 + 2\bar{\sigma}_{44}'^2\right] \tag{18}$$

where $\bar{\sigma}'_{ij} = \frac{\sigma'_{ij}}{S_{ij}}$. From above equation we can find that the yield criterion of the damaged orthotropic materials is isomorphic with the Von Mises criterion of isotropic materials.

According to Eq. (18), the equivalent active stress can be defined as

$$\bar{\sigma} = \frac{K}{\sqrt{2}}\sqrt{(\bar{\sigma}'_{11} - \bar{\sigma}'_{22})^2 + \bar{\sigma}'^2_{22} + \bar{\sigma}'^2_{11} + 2\bar{\sigma}'^2_{44}} \tag{19}$$

where the constant K can be determined by the tension test in simple stress state.

Let the yield function f be

$$f = \frac{k^2}{2}\left[(\bar{\sigma}'_{11} - \bar{\sigma}'_{22})^2 + \bar{\sigma}'^2_{22} + \bar{\sigma}'^2_{11} + 2\bar{\sigma}'^2_{44}\right] \tag{20}$$

where $\bar{\sigma}'_{ij} = \frac{\sigma_{ij} - b_{ij}}{S_{ij}}$ (i,j not sum).

According to Eqs. (15) and (20), the mixed hardening yield function can be given as

$$F_p = f(\bar{\sigma}'_{ij}) - [\bar{\sigma}(\bar{\varepsilon}^p)^2] \tag{21}$$

where the equivalent active stress $\bar{\sigma}$ is a function of the equivalent plastic strain $\bar{\varepsilon}^p$ and can be obtained by the simple tension test curves $\sigma - \varepsilon$.

Choose the plastic dissipation potential function to agree with the mixed hardening yield criterion. According to the orthogonality principle, we have

$$d\varepsilon^p_{ij} = \lambda_p \frac{\partial f}{\partial \sigma_{ij}} \tag{22}$$

where λ_p is a multiplier determined by continuity of the yield surface and will be deduced in the following processes. Substituting Eq. (20) into Eq. (22), the following equations can be obtained:

$$\begin{aligned} d\varepsilon^p_{11} &= \lambda_p \frac{K^2}{S_{11}}(2\bar{\sigma}'_{11} - \bar{\sigma}'_{22}) \\ d\varepsilon^p_{22} &= \lambda_p \frac{K^2}{S_{22}}(2\bar{\sigma}'_{22} - \bar{\sigma}'_{11}) \\ d\varepsilon^p_{44} &= 2\lambda_p \frac{K^2}{S_{44}}\bar{\sigma}'_{44} \end{aligned} \tag{23}$$

Substituting Eq. (23) into Eq. (19), we have

$$\begin{aligned} \bar{\sigma} = \frac{1}{3\sqrt{2}k\lambda_p}\Big\{&(S_{11}d\varepsilon^p_{11} - S_{22}d\varepsilon^p_{22})^2 + (S_{22}d\varepsilon^p_{22})^2 \\ &+ (S_{11}d\varepsilon^p_{11})^2 + \frac{9}{2}(S_{44}d\varepsilon^p_{44})^2\Big\}^{\frac{1}{2}} \end{aligned} \tag{24}$$

Define the equivalent plastic strain increment as

$$\begin{aligned} d\bar{\varepsilon}^p = \frac{\sqrt{2}}{3k}\Big\{&(S_{11}d\varepsilon^p_{11} - S_{22}d\varepsilon^p_{22})^2 + (S_{22}d\varepsilon^p_{22})^2 \\ &+ \left(S_{11}d\varepsilon^p_{11}\right)^2 + \frac{9}{2}(S_{44}d\varepsilon^p_{44})^2\Big\}^{\frac{1}{2}} \end{aligned} \tag{25}$$

The incremental plastic strain can be divided into two parts, $d\varepsilon^{p(i)}_{ij}$ and $d\varepsilon^{p(j)}_{ij}$, i.e. $d\varepsilon^p_{ij} = d\varepsilon^{p(i)}_{ij} + d\varepsilon^{p(j)}_{ij}$. Here $d\varepsilon^{p(i)}_{ij}$ is the incremental plastic strain related to the isotropic hardening, and $d\varepsilon^{p(j)}_{ij}$ is the incremental plastic strain related to kinematic hardening. They can be defined as $d\varepsilon^{p(i)}_{ij} = \alpha d\varepsilon^p_{ij}$, $d\varepsilon^{p(j)}_{ij} = (1-\alpha)d\varepsilon^p_{ij}$, here α is the mixed hardening parameter with span $(-1,1)$.$\alpha = 1(d\varepsilon^{p(j)}_{ij} = 0, d\varepsilon^p_{ij} = d\varepsilon^{p(i)}_{ij})$ denotes the isotropic hardening, and $\alpha = 0(d\varepsilon^{p(i)}_{ij} = 0,\ d\varepsilon^p_{ij} = d\varepsilon^{p(j)}_{ij})$ denotes the kinematic hardening. When α is negative the yield surface shrinks, and α with other values denotes mixed hardening. The incremental back stress tensor can be defined as a linear function of the incremental plastic strain tensor, that is

$$db_{ij} = cd\varepsilon^{p(j)}_{ij} = c(1-\alpha)d\varepsilon^p_{ij} \tag{26}$$

in which c is a ratio constant.

2.3.2. Elasto-plastic damage constitutive relations for orthotropic composite shallow spherical shell

With the above deduced mixed hardening rule for the orthotropic material, we work to establish an elasto-plastic damage constitutive relation for orthotropic composite shallow spherical shell in this part.

Suppose the total incremental strain is composed of two parts

$$d\varepsilon_{ij} = d\varepsilon^e_{ij} + d\varepsilon^p_{ij} \tag{27}$$

From Eqs. (22) and (27), Eq. (14) can be written as

$$d\sigma_{ij} = c^e_{ijkl}\left(d\varepsilon_{ij} - \lambda_p \frac{\partial f}{\partial \sigma_{ij}}\right) \tag{28}$$

Using the consistency conditions, from Eq. (21), we have

$$\frac{\partial f}{\partial \bar{\sigma}'_{ij}}d\bar{\sigma}'_{ij} - 2\bar{\sigma}\frac{\partial \bar{\sigma}}{\partial \bar{\varepsilon}^p}d\bar{\varepsilon}^p = 0 \tag{29}$$

here, $\bar{\sigma}$ is a function of the equivalent plastic strain $\bar{\varepsilon}^p$ as defined in Eq. (21).

Substituting Eqs. (22), (26) and (28) into (29), and using the (24) and (25), the multiplier λ_p can be obtained as

$$\lambda_p = \frac{\frac{\partial f}{\partial \bar{\sigma}'_{ij}}\frac{1}{S_{ij}}c^e_{ijkl}d\varepsilon_{ij}}{\frac{\partial f}{\partial \bar{\sigma}'_{ij}}\frac{1}{S^2_{ij}}c(1-\alpha)\frac{\partial f}{\partial \bar{\sigma}'_{ij}} + \frac{1}{S_{ij}}\frac{\partial f}{\partial \bar{\sigma}'_{ij}}c^e_{ijkl}\frac{1}{S_{kl}}\frac{\partial f}{\partial \bar{\sigma}'_{kl}} + 2\bar{\sigma}\frac{\partial \bar{\sigma}}{\partial \bar{\varepsilon}^p}\frac{1}{S_{ij}}\frac{\partial f}{\partial \bar{\sigma}'_{ij}}} \tag{30}$$

Substituting Eq. (30) into Eq. (28) and rearranging, the incremental elasto-plastic damage constitutive equation for orthotropic composite materials can be obtained

$$d\sigma_{ij} = (c^e_{ijkl} - \beta c^p_{ijkl})d\varepsilon_{kl} \stackrel{def}{=} Q_{ijkl}d\varepsilon_{kl} \tag{31}$$

where $c^p_{ijkl} = \frac{\frac{\partial f}{\partial \bar{\sigma}'_{ij}}\frac{1}{S_{ij}}c^e_{ijkl}\frac{\partial f}{\partial \bar{\sigma}'_{kl}}\frac{1}{S_{kl}}c^e_{klij}}{\frac{\partial f}{\partial \bar{\sigma}'_{ij}}\frac{1}{S^2_{ij}}c(1-\alpha)\frac{\partial f}{\partial \bar{\sigma}'_{ij}} + \frac{1}{S_{ij}}\frac{\partial f}{\partial \bar{\sigma}'_{ij}}c^e_{ijkl}\frac{1}{S_{kl}}\frac{\partial f}{\partial \bar{\sigma}'_{kl}} + 2\bar{\sigma}\frac{\partial \bar{\sigma}}{\partial \bar{\varepsilon}^p}\frac{1}{S_{ij}}\frac{\partial f}{\partial \bar{\sigma}'_{ij}}}$.

The yield conditions for the orthotropic composite material are

$$\begin{aligned} &\beta = 1 \text{ (elasto-plastic deformation) when } F_p = 0 \text{ and } \\ &\quad \frac{\partial f}{\partial \sigma_{ij}}d\sigma_{ij} > 0 \\ &\beta = 0 \text{ (elastic deformation) when } F_p < 0, \text{ or } F_p = 0 \text{ and } \frac{\partial f}{\partial \sigma_{ij}}d\sigma_{ij} \leqslant 0 \end{aligned} \tag{32}$$

As for the composite laminated shallow spherical shells, from the Eq. (31), we briefly denote the incremental elasto-plastic constitutive relations for the kth lamina of the laminated shallow spherical shell in the local coordinates

$$d\boldsymbol{\sigma}^{(k)} = \mathbf{Q}^{(k)} \cdot d\boldsymbol{\varepsilon}^{(k)} \tag{33}$$

where

$$\mathbf{Q} = \begin{bmatrix} C^e_{11} - \alpha_1 C^p_{11} & C^e_{12} - \alpha_1 C^p_{12} & -\alpha_1 C^p_{14} \\ C^e_{21} - \alpha_1 C^p_{21} & C^e_{22} - \alpha_1 C^p_{22} & -\alpha_1 C^p_{24} \\ -\alpha_1 C^p_{14} & -\alpha_1 C^p_{24} & C^e_{44} - \alpha_1 C^p_{44} \end{bmatrix}$$

in which the C^e_{ij} are determined by the Eq. (13).

The incremental stress $d\boldsymbol{\sigma}^{(k)}$ in the local coordinate can be transformed to the incremental stress $d\bar{\boldsymbol{\sigma}}^{(k)}$ in the global coordinate

$$d\boldsymbol{\sigma}^{(k)} = \mathbf{T}^{(k)}_{\sigma} \cdot d\bar{\boldsymbol{\sigma}}^{(k)} \tag{34}$$

The strain can be transformed by

$$d\boldsymbol{\varepsilon}^{(k)} = \boldsymbol{T}_{\varepsilon}^{(k)} \cdot d\bar{\boldsymbol{\varepsilon}}^{(k)} \tag{35}$$

$T_{\sigma}^{(k)}$ and $T_{\varepsilon}^{(k)}$ are the stress and strain transformation matrix, and can be written as

$$\boldsymbol{T}_{\sigma}^{(k)(-1)} = \boldsymbol{T}_{\varepsilon}^{(k)} \tag{36}$$

$$\boldsymbol{T}_{\varepsilon}^{(k)} = \begin{bmatrix} \cos^2\vartheta & \sin^2\vartheta & 0 \\ \sin^2\vartheta & \cos^2\vartheta & 0 \\ 0 & 0 & \cos\vartheta \end{bmatrix} \tag{37}$$

where ϑ is the angle between the local coordinate with the global coordinate. Then the incremental elasto-plastic damage constitutive equation for the kth lamina of the laminated shallow spherical shell can be obtained in the global coordinate as

$$d\bar{\boldsymbol{\sigma}}^{(k)} = \boldsymbol{T}_{\varepsilon}^{(k)T} \cdot \boldsymbol{Q}^{(k)} \cdot \boldsymbol{T}_{\varepsilon}^{(k)} \cdot d\bar{\boldsymbol{\varepsilon}}^{(k)} = \overline{\boldsymbol{Q}}^{(k)} \cdot d\bar{\boldsymbol{\varepsilon}}^{(k)} \tag{38}$$

2.4. Nonlinear motion equations of orthotropic laminated composite shallow spherical shells

Denote the membrane stress resultants of the laminated shallow spherical shell as N_{φ}, N_{θ}, the stress couples as M_x, M_y and the transverse shear force as Q_{φ}. The corresponding incremental components can be expressed as $dN_{\varphi}, dN_{\theta}, dN_{\varphi}, dN_{\theta}, dQ_{\varphi}$. According to the nonlinear classical flat shell theory presented in Fu (1997), and neglecting the plane inertia and rotational inertia, the nonlinear motion equations for the symmetrical cross-ply laminated moderately thick shallow spherical shells can be written as follows

$$\begin{aligned}
&(dN_{\varphi} - dN_{\theta}) + r\frac{\partial dN_{\varphi}}{\partial r} = 0 \\
&\frac{1}{r}\Big[dQ_{\varphi} - w_2 dN_{\varphi} - dw_2 N_{\varphi} - dw_2 dN_{\varphi}. \\
&\quad + r\frac{\partial}{\partial r}(dQ_{\varphi} - w_2 dN_{\varphi} - dw_2 N_{\varphi} - dw_2 dN_{\varphi})\Big] \\
&\quad + \frac{dN_{\varphi} + dN_{\theta}}{R} + dq \cdot \delta(r-0) = \rho h dw_{,tt} \\
&\frac{1}{r}\left(dM_{\varphi} - dM_{\theta} + r\frac{\partial dM_{\varphi}}{\partial r}\right) - dQ_{\varphi} = 0
\end{aligned} \tag{39}$$

The incremental membrane stress resultants dN_x, dN_y, the incremental stress couples dM_x, dM_y and the incremental transverse shear force dQ_{φ} can be obtained by using the Eqs. (2), (4) and (31)

$$\begin{aligned}
[dN_{\varphi}\ dN_{\theta}] &= \sum_{k=1}^{N}\int_{z_{k-1}}^{z_k} [d\sigma_{\varphi}^{k}\ d\sigma_{\theta}^{k}]dz \\
&= \begin{bmatrix} A_{11} & A_{12} & A_{14} \\ A_{12} & A_{22} & A_{24} \end{bmatrix} \begin{Bmatrix} d\varepsilon_{\varphi}^{0} \\ d\varepsilon_{\theta}^{0} \\ d\varepsilon_{\varphi z} \end{Bmatrix} + \begin{bmatrix} B_{11} & B_{12} \\ B_{12} & B_{22} \end{bmatrix} \begin{Bmatrix} d\kappa_{\varphi}^{0} \\ d\kappa_{\theta}^{0} \end{Bmatrix} \\
[dM_{\varphi}\ dM_{\theta}] &= \sum_{k=1}^{N}\int_{z_{k-1}}^{z_k} [d\sigma_{\varphi}^{k}\ d\sigma_{\theta}^{k}]zdz \\
&= \begin{bmatrix} B_{11} & B_{12} & B_{14} \\ B_{12} & B_{22} & B_{24} \end{bmatrix} \begin{Bmatrix} d\varepsilon_{\varphi}^{0} \\ d\varepsilon_{\theta}^{0} \\ d\varepsilon_{\varphi z} \end{Bmatrix} + \begin{bmatrix} D_{11} & D_{12} \\ D_{12} & D_{22} \end{bmatrix} \begin{Bmatrix} d\kappa_{\varphi}^{0} \\ d\kappa_{\theta}^{0} \end{Bmatrix} \\
dQ_{\varphi} &= \sum_{k=1}^{N}\int_{z_{k-1}}^{z_k} d\tau_{\varphi z}dz = C_{44}d\varepsilon_{\varphi z}
\end{aligned} \tag{40}$$

where

$$\begin{aligned}
A_{ij} &= \sum_{k=1}^{N}\left(C_{ij}^{e(k)} - \alpha_1 C_{ij}^{p(k)}\right)(z_k - z_{k-1}), \\
B_{ij} &= \frac{1}{2}\sum_{k=1}^{N}\left(C_{ij}^{e(k)} - \alpha_1 C_{ij}^{p(k)}\right)(z_k^2 - z_{k-1}^2) \\
D_{ij} &= \frac{1}{3}\sum_{k=1}^{N}\left(C_{ij}^{e(k)} - \alpha_1 C_{ij}^{p(k)}\right)(z_k^3 - z_{k-1}^3) \\
C_{44} &= \sum_{k=1}^{N}\left(C_{13}^{e(k)} - \alpha_1 C_{13}^{p(k)}\right)(z_k - z_{k-1}) \stackrel{def}{=} \sum_{k=1}^{N} G_{13}^{(k)}(z_k - z_{k-1})
\end{aligned} \tag{41}$$

From the third term in Eq. (40), it can be noticed that the transverse shear stress is not continuous, but distributes as a trapezium along the thickness, and the transverse shear forces on the top and bottom of the shell are not zero. In order to eliminate this flaw, a modification of the transverse shear force is proposed by applying the residual energy theory as follows

$$C_{44} = \frac{4h^2}{9}\sum_{k=1}^{N}\frac{G_{13}^{(k)}}{h_k - h_{k-1} - 8(h_k^3 - h_{k-1}^3)/3h^2 + 16(h_k^5 - h_{k-1}^5)/5h^4} \tag{42}$$

Introduce the following dimensionless parameters:

$$\begin{aligned}
&\bar{r} = \frac{r}{a}, \quad \lambda_1 = \frac{h}{a}, \quad \lambda_2 = \frac{a^2}{Rh}, \quad \lambda_4 = \frac{E_2}{E_1}, \quad \lambda_5 = \frac{G_{13}}{E_1}, \\
&\lambda_6 = \frac{G_{23}}{E_1}, \quad \bar{z} = \frac{z}{a}, \quad \overline{A}_{ij} = \frac{A_{ij}(1 - v_{12}v_{21})}{E_1 h}, \\
&\overline{D}_{ij} = \frac{D_{ij}(1 - v_{12}v_{21})}{E_1 h^3}, \quad dU = \frac{du^0 a}{h^2}, \quad dW = \frac{dw}{h}, \\
&d\psi = d\psi_1\frac{a}{h}, \quad \overline{G} = \frac{C_{44}a^2(1 - v_{12}v_{21})}{E_1 h^3}, \quad \overline{q} = \frac{q(1 - v_{12}v_{21})}{E_1\lambda_1^4}, \\
&\tau = t\sqrt{\frac{E_1\lambda_1^4}{\rho_0 h^2(1 - v_{12}v_{21})}}
\end{aligned} \tag{43}$$

Substituting Eqs. (40), (2), (3) and (43) into Eq. (39), the dimensionless nonlinear incremental governing equations of the cross-ply laminated moderately thick shallow spherical shell can be obtained in terms of dU, dW and $d\psi$.

In present study, the initial conditions are set as

$$d\overline{W}(\bar{r}, 0) = d\overline{W}_{,\tau}(\bar{r}, 0) = 0 \tag{44}$$

Supposing the moderately thick shallow spherical shells are completely restricted along the normal direction, but can partially rotate and move in the plane, the boundary conditions on the bottom and symmetrical conditions on the top are given as follows

$$\bar{r} = 0: \quad dU = 0, \quad dW_{,\bar{r}} = 0, \quad d\bar{\psi}_1 = 0 \tag{45a}$$

$$\begin{aligned}
\bar{r} = 1: \quad &\overline{A}_{11}(dU_{,\bar{r}} - \lambda_2 dW + \tfrac{1}{4}(dW_{,\bar{r}} - d\psi)(W_{,\bar{r}} - \psi) \\
&+\tfrac{1}{8}(dW_{,\bar{r}} - d\psi)^2) + \\
&\overline{A}_{12}\left(\tfrac{dU}{\bar{r}} - \lambda_2 dW\right) = -\overline{K}_i dU \\
&\overline{D}_{11}d\psi_{,\bar{r}} + \overline{D}_{12}\tfrac{d\psi}{\bar{r}} = \overline{K}_b dW_{,\bar{r}}(1) \\
&dW = 0
\end{aligned} \tag{45b}$$

where $\overline{K}_i = \frac{aK_i(1 - v_{12}v_{21})}{E_1 h}, \overline{K}_b = \frac{aK_b(1 - v_{12}v_{21})}{E_1 h^3}$, and K_i, K_b are the in-plane elastic strength and the rotary strength. $K_i = 0, \infty$ and $K_b = 0, \infty$ indicate the movable, unmovable, simple supported and clamped boundary conditions, respectively.

3. Solution methodology

3.1. Calculation of the contact force

Consider the shell is impacted by an elastic sphere on the top with a velocity of v_0. For a better understanding of the low velocity impact, divide the elasto-plastic impact into following three phrases:

(1) elastic loading

According to the yield criterion Eq. (32), when only elastic deformation occurs in contact area, the contact force and the Hertz contact pressure distribution as proposed in Liu and Somasak (1997) and Her and Liang (2004), can be given as

$$F(t)=\frac{4}{3}E^*\sqrt{R^*}\delta(t)^{\frac{3}{2}},\quad p(r)=\frac{3F}{2\pi a^2}\left[1-\left(\frac{r}{a}\right)^2\right]^{1/2} \tag{46}$$

where δ is the indentation; R^* and E^* are the equivalent contact curvature and equivalent Young's modulus, respectively, and $R^*=\left(\frac{1}{R}+\frac{1}{R'}\right)^{-1}, E^*=\left[\frac{(1-\nu'^2)}{E'}+\frac{(1-\nu^2)}{E}\right]^{-1}$; R, E, ν, R', E', ν' are the radius, Young's modulus and Poisson's ratio of the shallow spherical shell and the elastic impacting sphere. As for the orthotropic composite material, the E^* is modified as

$$E^*=\left[\frac{(1-\nu'^2)}{E'}+\frac{1}{E_z}\right]^{-1} \tag{47}$$

where E_z is the Young's modulus along the thickness direction.

(2) plastic loading

In order to model the post-"yield" behavior of the laminated composite shallow spherical shell, it is necessary to make some simplifying assumptions. If plastic deformation occurs, we assume a Hertzian pressure distribution with a cut-off corresponding to the contact yield contact pressure. Based on this assumption, Vu-Quoc et al. (2001) proposed a NFD contact model for the elasto-perfectly plastic material and regarded the contact pressure in the plastic region no longer increase after yield. As for the elasto-plastic material, it can be seen from the previous deduction of the elasto-plastic constitutive relations, the stresses continue to increase after yield and the equivalent active stress $\bar{\sigma}$, to which the plastic deformation is related, can reflect the plastic deformation level in the structure. In order to get a comparison with the $\bar{\sigma}$, an equivalent active stress σ^e related only to the elastic deformation is defined as follows

$$\sigma^e=\frac{k}{\sqrt{2}}\sqrt{\left[(\sigma_{11}-\sigma_{22})^2+\sigma_{22}^2+\sigma_{11}^2+2\sigma_{44}^2\right]} \tag{48}$$

where σ_{ij} can be determined by Eq. (13). Setting $\bar{\sigma}_{ij}=\frac{\sigma_{ij}}{S_{ij}}$, the Eq. (48) can be rewritten in dimensionless form as:

$$\bar{\sigma}^e=\frac{k}{\sqrt{2}}\sqrt{\left[(\bar{\sigma}_{11}-\bar{\sigma}_{22})^2+\bar{\sigma}_{22}^2+\bar{\sigma}_{11}^2+2\bar{\sigma}_{44}^2\right]} \tag{49}$$

Therefore, after yield, the normal contact force can be given by

$$F=F_e-2\pi\int_0^{a_p}[p(r)-\lambda p_y]rdr \tag{50}$$

where $\lambda=\frac{\bar{\sigma}^e-\bar{\sigma}}{\bar{\sigma}_y^e-\bar{\sigma}_y}$; $\bar{\sigma}_y^e, \bar{\sigma}_y$ are the yield equivalent active stress; F_e is the equivalent elastic force given by Eq. (46), which would result in the same total contact area and the integral upper limit a_p is the radius of the plastic area over which a uniform pressure is assumed as indicated in Fig. 2; p_y is the maximum contact pressure

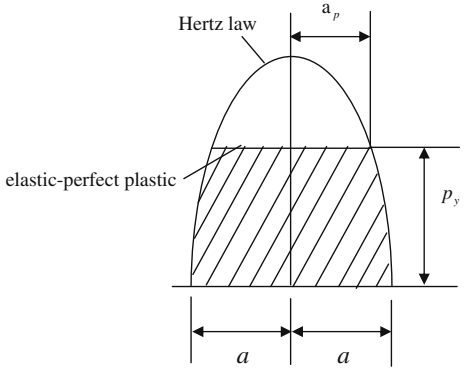

Fig. 2. Normal contact force distribution.

when yield occurs. It can be seen that when yield occurs, then $\lambda>1$, and λ is in proportion to the plastic deformation. For simplification, the $\bar{\sigma}, \bar{\sigma}_y, \bar{\sigma}^e$ and $\bar{\sigma}_y^e$ are chosen as the value at the center point in the contact area and regarded as constants all over the contact area.

The integral of the Eq. (50) gives

$$F=\lambda\pi a_p^2 p_y+\frac{4E^*R^{*1/2}}{3}\delta^{3/2}\left[1-\left(\frac{a_p}{a}\right)^2\right]^{3/2} \tag{51}$$

There exists the following relation after yield occurs in the contact area

$$a^2=a_p^2+a_y^2 \tag{52}$$

where a is the radius of the contact area, and a_y is the radius of the contact area when yield occurs

Substituting Eq. (52) into (51) and using the Hertzian transition $a^2=R^*\delta$, we obtain

$$F=F_y+\lambda p_y R^*(\delta-\delta_y) \tag{53}$$

where δ_y is the yield indentation.

(3) elastic unloading

If plastic deformation occurs during the loading stage, the contact curvature during unloading is $1/R_p^*<1/R^*$ due to permanent deformation of the contact surfaces. During unloading the force–displacement behavior is assumed to be elastic and is provided by the Hertzian equations but with curvature $1/R_p^*$ corresponding to the point of maximum compression. At the point of unloading, the contact area developed by the actual maximum normal force and the reduced curvature $1/R_p^*$ is the same as that which would be generated by an equivalent elastic force P_e^* and a contact curvature $1/R^*$.

Hence, the following relation can be obtained

$$R_p^*P^*=R^*P_e^* \tag{54}$$

And the contact force can be obtained during elastic unloading as

$$F(t)=\frac{4}{3}E^*\sqrt{R_p^*}(\delta(t)-\delta_p(t))^{\frac{3}{2}} \tag{55}$$

where $R_p^*=\frac{4E^*}{3P^*}\left(\frac{2P^*+P_y}{2\pi\sigma_y}\right)^{3/2}$, $\delta_p(t)$ is defined in Fig. 3.

When the elastic sphere impacts on the top of the shallow spherical shell along the normal direction at the velocity v_0 (as shown in the Fig. 4), the indentation δ during the impact can be obtained by

$$\delta(t)=s(t)-w(0,t) \tag{56}$$

where $s(t)$ is the displacement of the impacting sphere after contact with the shells, $w(0,t)$ is the displacement of the shell at the impact

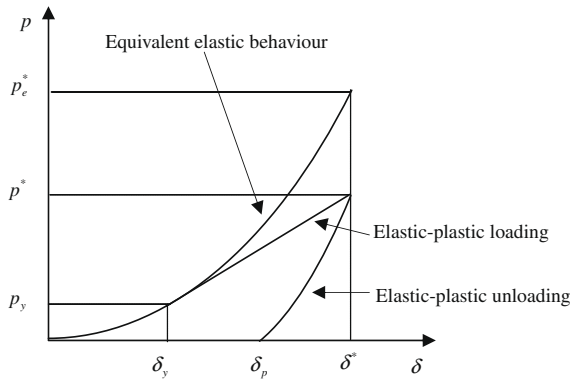

Fig. 3. Force–displacement relationship.

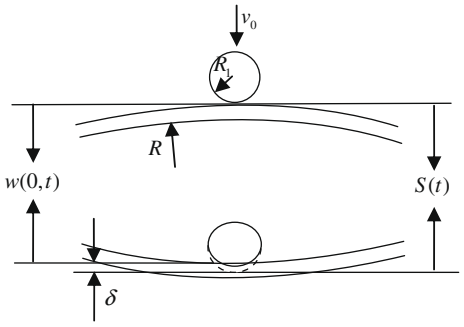

Fig. 4. Local deformation at the point of contact.

point $(r = 0)$ due to the impact. Suppose that at the just moment of contact the displacement is zero, then

$$s(t) = v_0 t - \frac{1}{m}\int_0^t dt \int_0^t F(t)dt \tag{57}$$

$$\delta(t) = v_0 t - \frac{1}{m}\int_0^t dt \int_0^t F(t)dt - w(0,t) \tag{58}$$

Obviously, it is impossible to obtain the analytic solution of the Eq. (58). Therefore the time increment method is applied to linearize the impact force by considering the contact force $F(t)$ to be constant during each Δt. At each time incremental interval $[t_n, t_{n+1}] = [n\Delta t, (n+1)\Delta t]$, the Eq. (58) can be written as follows

$$\delta(t) = v_0 n\Delta t - \frac{1}{m'}(\Delta t)^2 \sum_{i=1}^{n} D_{n-i+1}F_i - w(0,t) \tag{59}$$

where the second item on the right can be deduced from the second integral item on the right of the Eq. (58), which can be written as

$$\sum_{i=1}^{n} D_{n-i+1}P_i = 2\sum_{i=1}^{n}(n-i)\sum_{j=1}^{i}(-1)^{i-j}P_j + \frac{1}{3}\sum_{i=1}^{n}(-1)^{n-i}P_i \tag{60}$$

Assuming at the moment the object contacts with the shallow spherical shells the local deformation mainly exists in the contact area, the initial contact force deduced from the Eq. (46) in the iterative process can be obtained as $p_1 = \xi(v_0\Delta t)^{3/2}$ by neglecting the whole solid displacement of the structure. When the δ is obtained by Eq. (59) at each step, the contact force can be calculated out by substituting the δ into Eq. (46) or (53). The substitution of the δ depends on the yield condition Eq. (32). The contact force also can be obtained by the Eq. (55) in the unloading state.

To seek approximate solution to the nonlinear incremental motion equations of the elasto-plastic laminated shallow spherical shell, the displacement functions dU, dW and $d\varphi$ are separated both for space and time by orthogonal collocation point method and Newmark method.

The following *Chebyshev* polynomials are chosen

$$\bar{r}_i = \frac{1}{2}\left\{1 + \cos\left[\frac{(2i-1)\pi}{2M}\right]\right\}, \quad i = 1, 2, \ldots, M \tag{61}$$

Define the numerical value at inner and outer collocation point as $\bar{r}_{M+1} = 0, \bar{r}_0 = 1$. The variable functions are expanded in series as follows

$$dU(\bar{r}) = \sum_{j=1}^{M+2}\bar{r}^{j+1}a_j, \quad dW(\bar{r}) = \sum_{l=1}^{M+2}\bar{r}^{l+1}c_l,$$
$$d\psi(\bar{r}) = \sum_{n=1}^{M+2}\bar{r}^{n+1}b_n, \ 0 \leqslant \bar{r} \leqslant 1 \tag{62}$$

The time is equally divided into small time segment Δt, and the whole equations are iterated to seek solutions. At each step of iteration, the nonlinear items in the equations and boundary conditions are linearized. For example, at the step j, the nonlinear items may be transformed to

$$(x \cdot y)_J = (x)_J \cdot (y)_{J_p} \tag{63}$$

where $(y)_{J_p}$ is the average value of those obtained in the preceding two iterations. For the initial step of the iteration, it can be determined by using the quadratic extrapolation, i.e.

$$(y)_{J_p} = A(y)_{J-1} + B(y)_{J-2} + C(y)_{J-3} \tag{64}$$

The coefficient $(y)_{J_p}$ can be evaluated at different iterative steps as follows

$$\begin{aligned} &J = 1 : A = 1, \ B = 0, \ C = 0 \\ &J = 2 : A = 2, \ B = -1, \ C = 0 \\ &J \geqslant 3 \ \ : A = 3, \ B = -3, \ C = 1 \end{aligned} \tag{65}$$

Moreover, the iteration item in the equations can be written as follows by using the Newmark scheme

$$(W_{,\tau\tau})_J = \frac{4(W_J - W_{J-1})}{(\Delta\tau)^2} - \frac{4(W_{,\tau})_{J-1}}{\Delta\tau} - (W_{,\tau\tau})_{J-1}$$
$$(W_{,\tau})_J = (W_{,\tau})_{J-1} + \frac{1}{2}[(W_{,\tau\tau})_J + (W_{,\tau\tau})_J](\Delta\tau) \tag{66}$$

Using Eqs. (62), (63) and (66), the governing equation and boundary conditions (45) can be transformed to a series of linear equations at each collocation point, and the solutions to these $3M + 6$ linear equations can be acquired with the initial conditions (44). For each time step, the iteration lasts until the difference of the present value and the former is smaller than 0.1%. In the present analysis, the initial damage value of the structure is considered to be zero. When the convergent solution in the Jth step is held, the damage value at the inner and outer boundary points in conjunction with other M points in the shells can be calculated out by using Eqs. (5), (6), (7), (9) and (10). They are to be used at the $J + 1$th step. The following finite difference format is chosen to deal with the differential items of the damage at the inner boundary and other collocation points

$$d_{j,\bar{r}}(\bar{r}_i) = \frac{d_j(\bar{r}_{i-1}) - d_j(\bar{r}_i)}{\bar{r}_{i-1} - \bar{r}_i}, \quad (j = 1, 2 \quad i = 1, 2, \ldots, M+1) \tag{67}$$

4. Numerical results

To verify validity of the present elasto-plastic impact model, a comparison with Johnson (1985) is carried out. According to Johnson (1985), for an elasto-plastic half space indented by a projectile

with spherical contact surface, the critical indentation δ_Y and the contact force $F(\delta)$ are given as

$$\delta_Y = \left(\frac{\pi\theta_Y Y R_*}{K_h}\right) \tag{68}$$

$$F(\delta) = K_h\delta^{3/2} \tag{69}$$

where Y is the yield stress of the softer material, θ_Y is the ratio of mean contact yield pressure to the uniaxial yield stress. Johnson (1985) has examined different geometries of contacting bodies to find this ratio. For the contact of spherical solids, $\theta_Y \approx 0.1$. K_h is the Hertz contact stiffness, given by

$$K_h = \frac{4}{3}E_*\sqrt{R_*} \tag{70}$$

E_* and R_* are the equivalent Young modulus and equivalent curvature, given by

$$\frac{1}{R_*} = \frac{1}{R_1} + \frac{1}{R_2} \quad \text{and} \quad \frac{1}{E_*} = \frac{1-\nu_1^2}{E_1} + \frac{1-\nu_2^2}{E_2} \tag{71}$$

In this comparing case, the material parameters of the shallow spherical shell are $E = 70$ GPa, Poisson's ratio $\mu = 0.33$, mass density $\rho = 2.768 \times 10^3$ kg/m^3; the material parameters of the impacting sphere are $E = 200$ GPa, $\mu = 0.33$, $\rho' = 7.9718 \times 10^3$ kg/m^3; the radius of the circular plate and the impacting sphere are $R_2 = 38$ mm, $R_1 = 19$ mm, respectively. When the Young modulus E_1 of the shell is changed, δ_Y, the minimum indentation required to initiate the plastic deformation, and the contact force $F(\delta_Y)$ obtained by the contact model presented in this paper are compared with that by the Eqs. (68) and (69) in Table 1. In Table 1, the δ_1 and F_1 are the results obtained by Eqs. (68) and (69), and the δ_2 and F_2 are results by present model. It can be seen these two results agree well and only small difference is observed, which proves the present method's feasibility.

The contact force $F(\delta)$ during the plastic–elastic indentation phase is given by Johnson (1985) as

$$F_2(\delta) = \left(\frac{2\delta}{\delta_Y} - 1\right)\left\{1 + \frac{1}{3\theta_Y}\ln\left(\frac{2\delta}{\delta_Y} - 1\right)\right\}F_1(\delta_Y) \tag{72}$$

where $F_1(\delta_Y)$ and δ_Y are critical contact force and indentation. Fig. 5 presents the comparison between the present results and that by Eq. (72) in the phase of the plastic initiation and propagation in the contacting zone. From Fig. 5, it can be found two results agree well when δ is small, but the difference becomes larger as the δ increases. Because in Johnson (1985) an elastic–perfectly plastic model is considered, while in present model, an elastic–plastic model is developed and the assumption is adopted that the bearing capacity in plastic zone still increases as the contact force rises.

In the following numerical examples, an eight-layer cross-ply $[90^\circ/0^\circ/0^\circ/90^\circ]_2$ laminated composite shallow spherical shell is considered. The material parameters are shown in Table 2. Except the particular indication, the geometric parameters of the laminated shallow spherical shell are set as: $a = 0.16$ m, $R = 5$ m, $h = 0.008$ m; the material parameters of the impacting sphere are: $E = 200$ GPa, $\nu = 0.3$, $\rho = 7.892 \times 10^3$ kg/m^3; and the radius of the impacting sphere is $R = 0.12$ m. In the presented results, W_0 represents the central dimensionless deflection of the shallow spherical shell and τ represents the dimensionless time.

Table 1
The comparison of critical indentation δ and contact force F with Johnson (1985).

E_1(GPa)	30	45	68.5	80	100	115	130
δ_1 (10^{-3} m)	8.374	7.163	6.377	6.180	5.939	5.815	5.721
δ_2 (10^{-3} m)	7.567	6.817	6.064	5.931	5.873	5.724	5.569
F_1 (MPa)	3.061	2.618	2.330	2.259	2.171	2.126	2.091
F_2 (MPa)	2.870	2.504	2.169	2.070	1.980	1.899	1.943

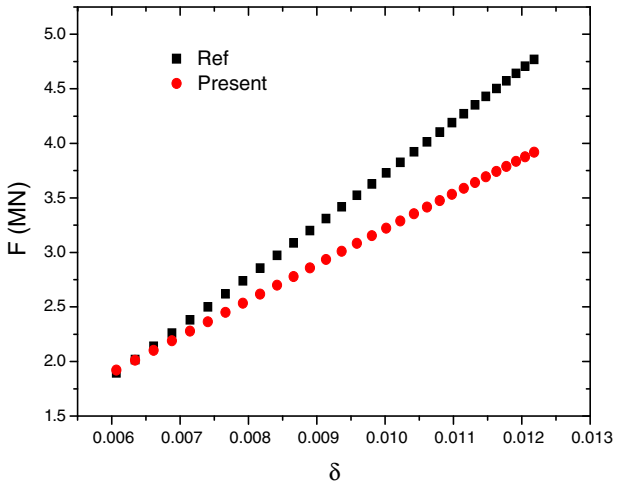

Fig. 5. Contact force in the elastic–plastic phase.

The dynamic response of the shallow spherical shell with clamped boundary condition and contact force when only elastic deformation is considered are compared with that when elasto-plastic deformation are considered. From Fig. 6, we can observe that the impact duration is greater when elasto-plastic behavior is considered. Because of the energy lose in plastic deformation the contact force for elastic case is greater than that for the elasto-plastic case, and consequently the contact force history for elasto-plastic case is asymmetric. We can also find the deflection of the structure for elasto-plastic contact case is greater than that for the elastic case due to the permanent plastic deformation.

Fig. 7 gives the dynamic response of the shell and the contact force when different velocities of the impacting sphere are set. It can be observed that the central deflection of the structure as well as the contact force increases as the velocity is greater. When the velocities are set as $v = 18$ m/s and $v = 12$m/s, the maximum deflections of the shallow spherical shell are 1.25404 and 0.5548 mm, and contact force are 135.55013 and 77.4542 kN, the contact duration are 1.57885 and 1.61557 ms. Conclusion that effect of the initial velocity of the impacting sphere on the deformation and contact force is greater than on the impact duration can be drawn. Obviously, the low velocity impact event is a problem with small deformation but great stress. Though only small deformation of the structure is observed when subjected to low velocity impact, a great inner stress may be caused. So the damage analysis of the structure under the low velocity impact is very important.

When the damage effect is in consideration, the damage parameters are taken as $k_1 = k_1 = 0.2$, $n_1 = n_2 = 2$, $A_1 = A_2 = 1$. The effect of damage on dynamic response of the elasto-plastic laminated shallow spherical shell with edge clamped and contact force are shown in Fig. 8. It can be observed that when the damage effect is considered, both of the contact force and the deflection of the structure become greater than the no damage case. That is because when the damage emerge and accumulate in the structure due to the impact, the structure' stiffness would be reduced, and consequently, the vibration amplitude of the structure and the contact force become larger, but the dynamic frequency decreases. It also can be found the time for the damage to emerge is advanced as the impacting velocity increases.

The stress components $(\sigma_{11}, \sigma_{22}, \tau_{13})$ of the central points in the first and second layers are illustrated in Fig. 9. From the figure, it can be found the stresses in the first lamina are greater than that in the second lamina. The transverse shear stress τ_{13} is smaller

Table 2
Material parameters of the composite shell.

E_1	E_2, E_3	υ_{12}	υ_{21}	G_{12}, G_{13}	G_{23}	X_T, X_C	Y_T	Y_C	S_i
109.34 GPa	8.82 GPa	0.342	0.028	4.32 GPa	3.2 GPa	1132 MPa	59 MPa	211 MPa	54 MPa

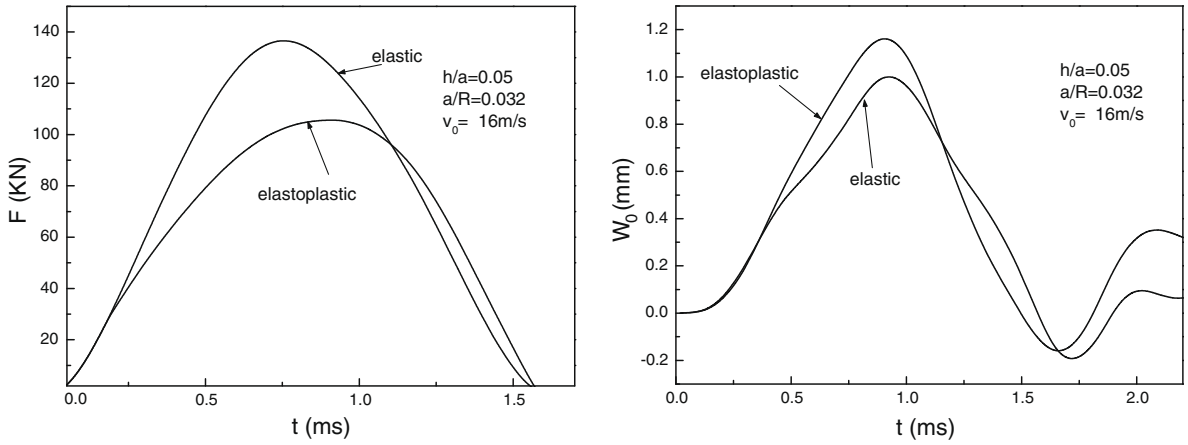

Fig. 6. Comparison of the dynamic response of the laminated shallow spherical shell with clamped boundary condition and contact force when elastic–plastic deformation and elastic deformation are in consideration, respectively.

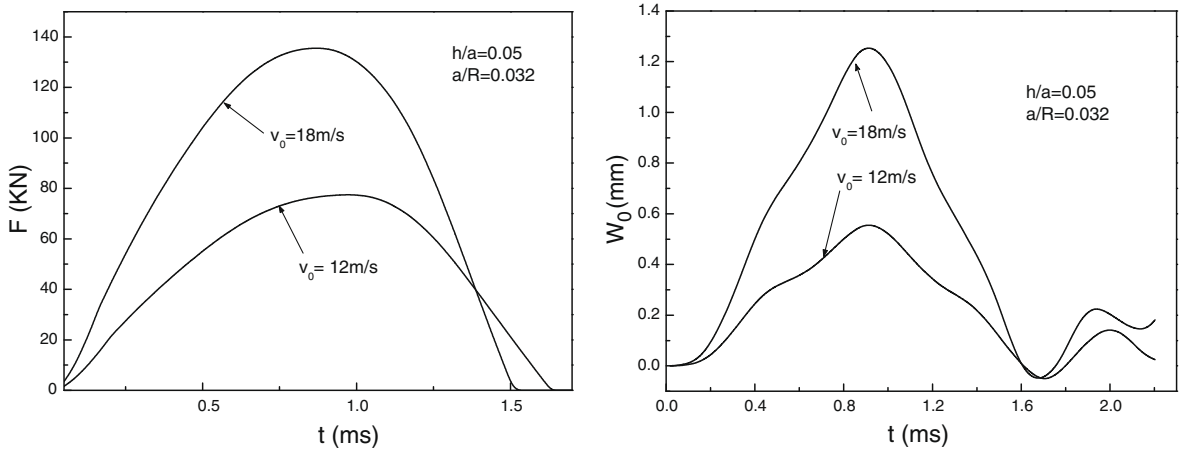

Fig. 7. Dynamic response curve for the elasto-plastic shallow spherical shell with clamped boundary condition and contact force when different initial velocities of the impacting sphere are set.

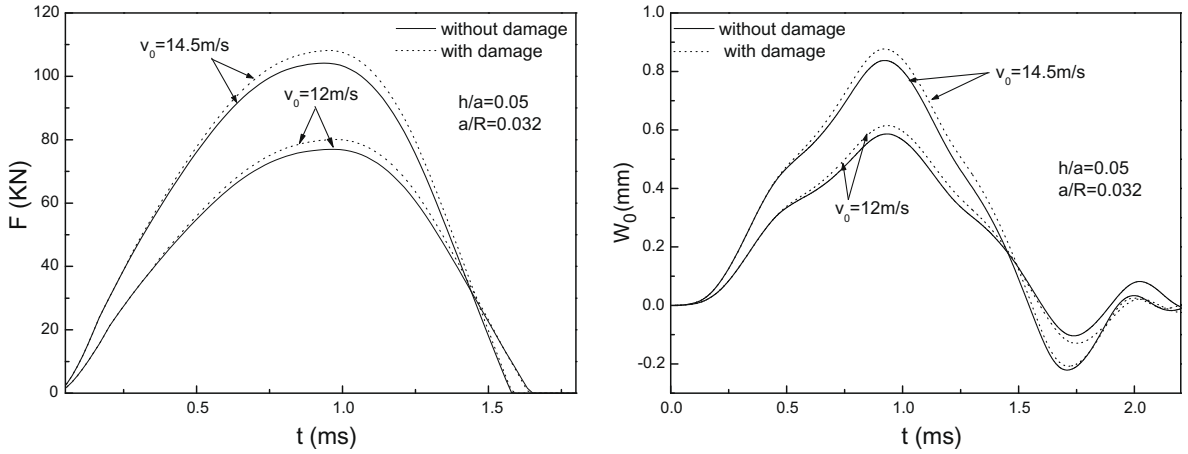

Fig. 8. Effect of the damage on the dynamic response and contact force of the laminated shallow spherical shell with clamped boundary condition when subjected to low velocity impact.

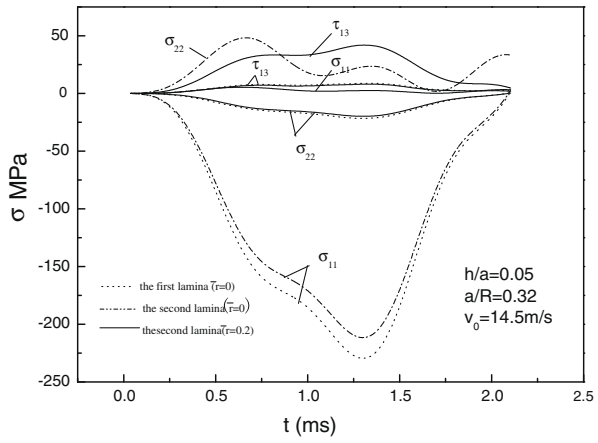

Fig. 9. Comparison of the stress distribution at different points.

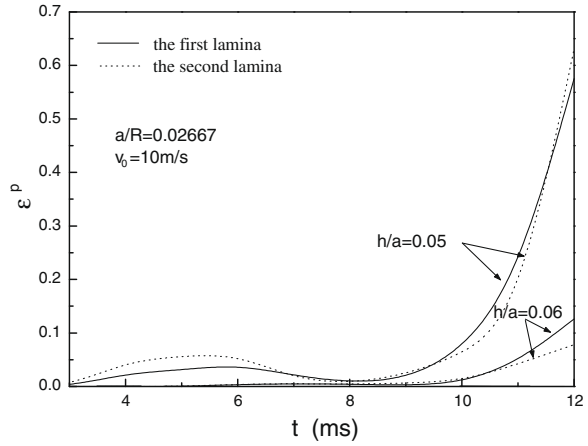

Fig. 11. Distribution of the equivalent plastic strain.

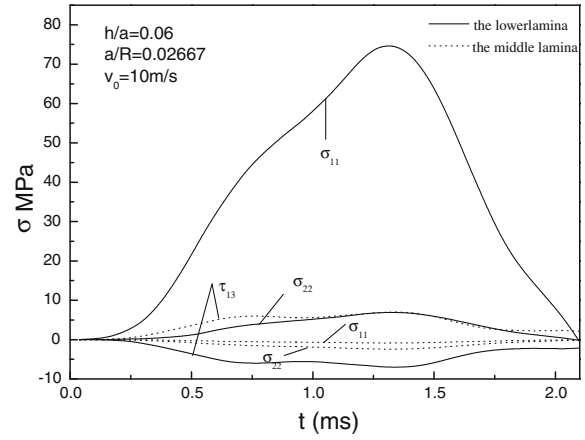

Fig. 12. Stress distribution at the lower and middle lamina.

than in-plane stresses σ_{11} and σ_{22}. All of the stress components at the point $(\bar{r} = 0.2)$ are comparatively small and the transverse shear force are greater than the rest of the stress components.

Fig. 10 illustrates the damage of different kinds in the first and second laminas along the $\bar{r}$ direction. The damage parameters d_{mn} indicate the nth type of damage in the $m(m = 1, 2)$ lamina. And n set as 1, 2, 3, denote the delamination, matrix crack and fiber–matrix shear failure, respectively. It can be seen from the figure that the maximum damage is the matrix crack in the vicinity of the contact point. Because the stress and strain are greatest in the first lamina (shown in Fig. 9) and correspondingly the damage threshold is firstly met, so the matrix crack firstly occurs in the top lamina underneath the contact point due to orthotropic property of the composite material, and then expands into the inner layer as the contact force increases. It also can be concluded from the data that fiber failure is comparatively small and the damage at the point away from the contact point is mainly the fiber–matrix shear failure caused by the transverse shear force where the transverse shear force dominates.

When the velocity of the impacting sphere is set as 10 m/s, Figs. 11 and 12 illustrate the equivalent plastic strains in the first and second laminas and the stress components in the lower and middle lamina. It can be observed from the Fig. 11 that the equivalent plastic strains in the first lamina are greater than that in the second lamina. The equivalent plastic strains at the center are much greater than that far away from the contact point. But the plastic deformation is in general small caused by the low velocity impact. From the Fig. 12, it can be demonstrated that the stresses in the last lamina (lower lamina) are negative whereas in the first lamina (top lamina) they are positive (shown in Fig. 9). The in-plane stresses components σ_{11}, σ_{22} at the mid-plane are neglected while the transverse shear force τ_{13} is not much neglected. This means that those two components contribute more to matrix crack damage compared with the other components. It also have been discovered the values of damage variables d_{12}, d_{11} are 0.401245 and 0 when elasto-plastic deformation is in consideration at the point underneath the contact point while they are 0.440455 and 0.052137 when only elastic deformation is considered. So it can be concluded that the plastic deformation would hamper the damage development.

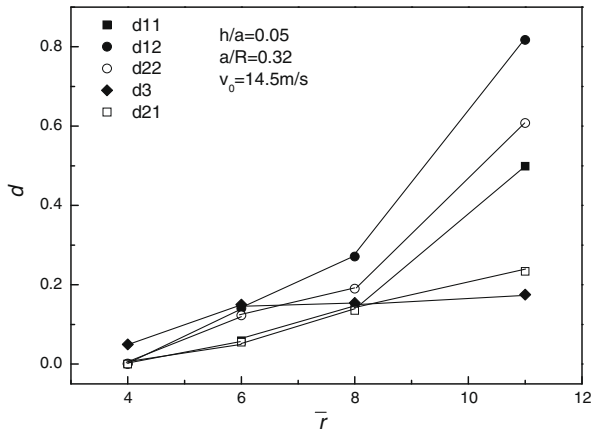

Fig. 10. Comparison of the different types of damage.

Fig. 13 shows the dynamic response of the structure and contact force when different base radius a are set. It can be noticed that the geometric size of the structure has an apparent effect on the dynamic response of the structure. When maintain the thickness of the structures and decrease the base radius a, the central deflection of the shallow spherical shell greatly decreases. The decrease of the contact force and slight increase of the impact duration can also be observed from the figure.

Fig. 14 presents the dynamic response and contact force when the radius of the impacting sphere changes. Set the radius of the impacting sphere as 0.09 m, and 0.105, respectively. It can be seen from the figure that when increase the radius of the impacting sphere, the central deflection of the structure and contact force increase, and impacting duration also increase apparently.

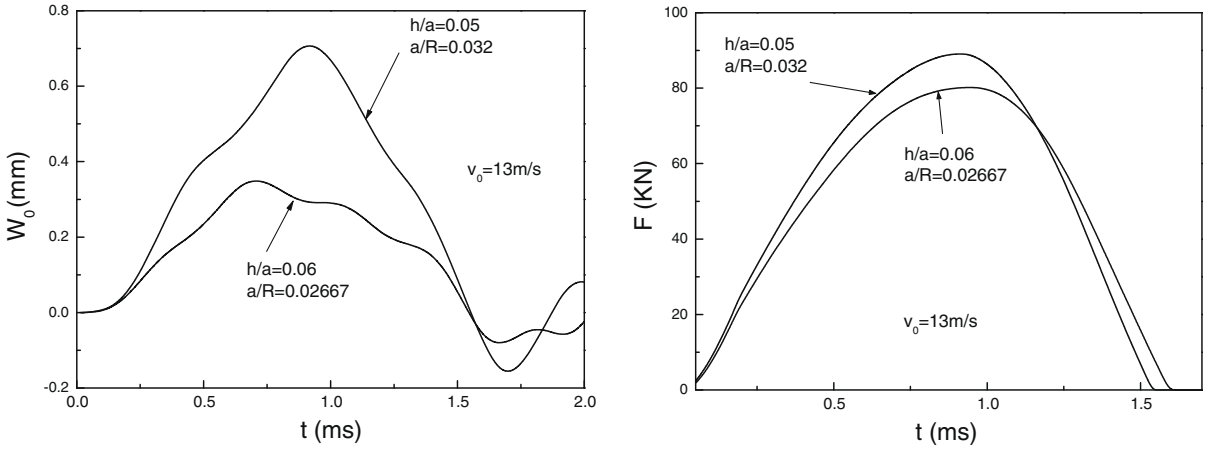

Fig. 13. Effect of the thickness-span ratio on the dynamic response of the laminated shallow spherical shell with clamped boundary condition and contact force.

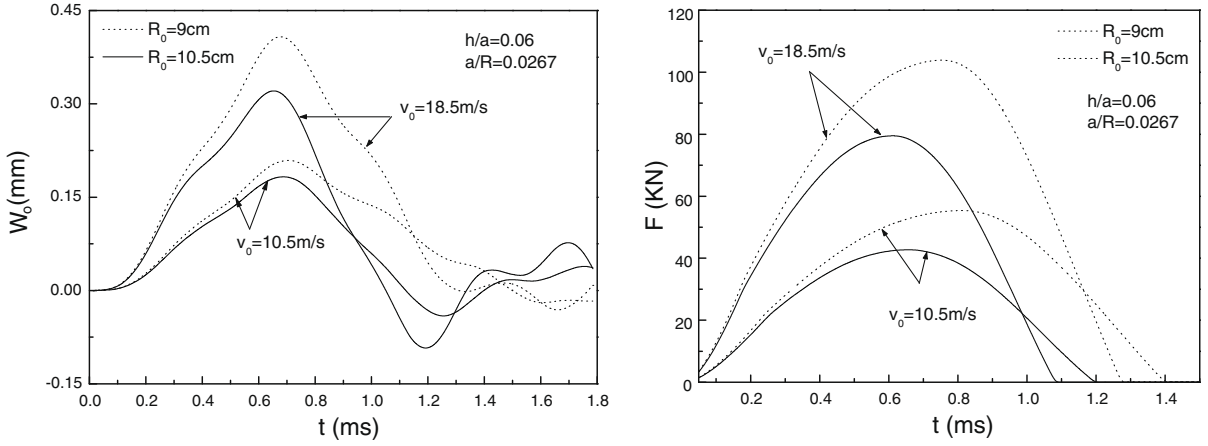

Fig. 14. Effect of the radius of the impacting sphere on the dynamic response of the laminated shallow spherical shell with clamped boundary condition and contact force.

A comparison between clamped $(k_i = \infty, k_b = \infty)$ and simply supported boundary conditions $(k_i = \infty, k_b = 0)$ for the laminated shallow spherical shell is shown in the Fig. 15. The velocity of impacting sphere is 14 m/s. When the structure is clamped the dynamic response of the structure and the contact force are greater than that when under simply supported boundary condition.

5. Conclusion

In this paper, a nonlinear dynamic and damage analytical model for the elasto-plastic laminated moderately thick shallow spherical shell under low velocity impact is proposed and the nonlinear dynamic response of the laminated shallow spherical shell, the dam-

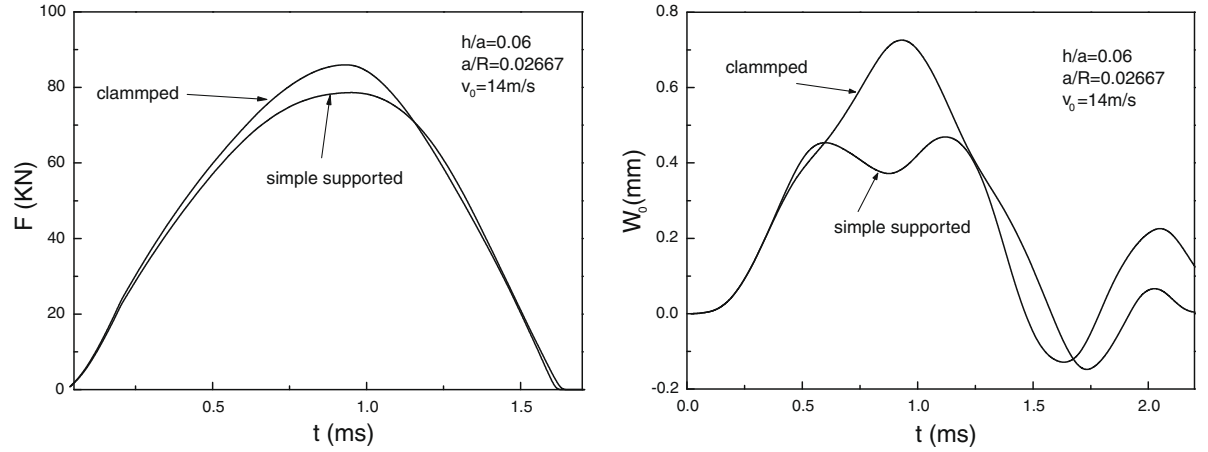

Fig. 15. Effect of the boundary condition on the dynamic response of the laminated shallow spherical shell and contact force.

age evolution and elasto-plastic deformation have been investigated. The numerical results are obtained by using orthotropic collocation point method and Newmark scheme. The main conclusions can be drawn as follows: when the elasto-plastic behavior is considered, the impact duration is greater but the contact force is smaller than that when only elastic behavior is considered; the dominating damage in contact area is matrix crack caused by in-plane stress, whereas the damage at the point away from the contact point is mainly caused by transverse shear force; damage reduces structure's stiffness and consequently decreases the response frequencies and increases the response amplitudes; the plastic deformation would hamper the damage development; the geometrical size of the impacting sphere and shallow spherical shell influence greatly the dynamic response of the shell and contact force.

Acknowledgement

This study is supported by the National Natural Science Foundation of China under Grant No. 10872066.

References

Chang, W.R., Etsion, I., Bogy, D.B., 1987. An elastic–plastic model for the contact of rough surfaces. ASME Journal of Tribology 109, 300–319.

Choi, H.Y., Chang, F.K., 1992. A model for predicting damage in graphite/epoxy laminated composites resulting from low-velocity point impact. Journal of Composite Materials 26 (14), 2134–2169.

Collombet, F., Bonini, J., Lataillade, J.L., 1996. A three-dimensional modeling of low velocity impact damage in composite laminates. International Journal for Numerical Methods in Engineering 39, 1491–1516.

Chien, H.H., Lee, Y.J., 2003. Experiments and simulation of the static contact crush of composite laminated plates. Composite Structures 61, 265–270.

Choi, I.H., Lim, C.H., 2004. Low-velocity impact analysis of composite laminates using linearized contact law. Composite Structures 66, 125–132.

Fu, Y.M., 1997. Nonlinear Dynamic Response Analysis of the Structure. Jinan University Press, Guangzhou.

Ganapathy, S., Rao, K.P., 1997. Interlaminar stress in laminated composite plates, cylindrical/spherical shell panels damaged by low-velocity impact. Composite Structures 38 (1–4), 156–168.

Hou, P.J., Petrinic, N., Ruiz, C., Hallett, S.R., 2000. Prediction of impact damage in composite plates. Composites Science and Technology 60, 273–281.

Her, S.C., Liang, Y.C., 2004. The finite element analysis of composite laminates and shell structures subjected to low velocity impact. Composite Structures 66, 277–285.

Johnson, K.L., 1985. Contact Mechanics, second ed. Cambridge University Press, New York.

Liu, Z.S., Somasak, S., 1997. Response of plate and shell structures due to low velocity impact. Journal of Engineering Mechanics.

Plantard, G., Papini, M., 2005. Mechanical and electrical behaviors of polymer particles. Experimental study of the contact area between two particles. Experimental validation of a numerical model. Granular Matter 7 (1), 1–12.

Sun, C.T., 1977. An analytical method for evaluation of impact damage energy of laminated composites. ASTM STP 617, 427–440.

Tam, T.M., Sun, C.T., 1982. Wave propagation in graphite/epoxy laminates due to impact. NASA CR 168057.

Vu-Quoc, L., Zhang, X., 1999. An Elasto-Plastic contact force–displacement model in the normal direction: displacement-driven version. Proceedings of the Royal Society of London, Series A 455 (1991), 4013–4044.

Vu-Quoc, L., Zhang, X., Lesburg, L., 2000. A normal force–displacement model for contacting spheres, accounting for plastic deformation: force-driven formation. ASME Journal of Applied Mechanics 67 (2), 363–371.

Vu-Quoc, L., Zhang, X., Lesburg, L., 2001. Normal and tangential force–displacement relations for frictional elasto-plastic contact of spheres. International Journal of Solids and Structures 38 (36–37), 6455–6589.

Vu-Quoc, L., Lesburg, L., Zhang, X., 2004. An accurate tangential force–displacement model for granular-flow simulations: contacting spheres with plastic deformation, force-driven formulation. Journal of Computational Physics 196 (1), 298–326.

Yang, S.H., Sun, C.T., 1981. Indentation law for composite laminates. ASTM STP 787, 425–449.

Zhang, Y., Lai, X.M., Zhu, P., Liang, X.H., 2006. Finite element analysis of low-velocity impact damage in composite laminated plates. Acta Material Composites Sinica 23 (2), 150–157.

Zhang, X., Vu-Quoc, L., 2007. An accurate elasto-plastic frictional tangential force–displacement model for granular flow simulations: displacement-driven formulation. Journal of Computational Physics 225 (1), 730–752.